Climate Dynamics
September 2010, Volume 35, Number 4, Pages 669-683
http://dx.doi.org/10.1007/s00382-009-0655-z

Low and high frequency Madden–Julian oscillations in austral summer: interannual variations

Takeshi Izumo[1, 2, *], Sébastien Masson[2], Jérome Vialard[2], Clément de Boyer Montegut[3], Swadhin K. Behera[1], Gurvan Madec[2], Keiko Takahashi[4] and Toshio Yamagata[1, 5]

[1] Institute For Global Change (JAMSTEC), Yokohama, Japan
[2] LOCEAN, IRD-CNRS-UPMC, Paris, France
[3] IFREMER, Brest, France
[4] Earth Simulator Center (JAMSTEC), Yokohama, Japan
[5] University of Tokyo, Tokyo, Japan

*: Corresponding author : Takeshi Izumo, email address : izumo@jamstec.go.jp

Abstract:

The Madden–Julian oscillation (MJO) is the main component of intraseasonal variability of the tropical convection, with clear climatic impacts at an almost-global scale. Based on satellite observations, it is shown that there are two types of austral-summer MJO events (broadly defined as 30–120 days convective variability with eastward propagation of about 5 m/s). Equatorial MJO events have a period of 30–50 days and tend to be symmetric about the equator, whereas MJO events centered near 8°S tend to have a longer period of 55–100 days. The lower-frequency variability is associated with a strong upper-ocean response, having a clear signature in both sea surface temperature and its diurnal cycle. These two MJO types have different interannual variations, and are modulated by the Indian Ocean Dipole (IOD). Following a negative IOD event, the lower-frequency southern MJO variability increases, while the higher-frequency equatorial MJO strongly diminishes. We propose two possible explanations for this change in properties of the MJO. One possibility is that changes in the background atmospheric circulation after an IOD favour the development of the low-frequency MJO. The other possibility is that the shallower thermocline ridge and mixed layer depth, by enhancing SST intraseasonal variability and thus ocean–atmosphere coupling in the southwest Indian Ocean (the breeding ground of southern MJO onset), favour the lower-frequency southern MJO variability.

Keywords: Intraseasonal Madden–Julian oscillation (MJO) - Seychelles–Chagos thermocline ridge/thermocline dome of the Indian Ocean - Indian Ocean dipole (IOD) - El Nino southern oscillation (ENSO) - Diurnal cycle - Oceanic diurnal warm layers - Air–sea interactions - Ocean–atmosphere coupling - Interannual variations - Mixed layer - Australian weather

1. Introduction

The Madden-Julian Oscillation (MJO) is the main component of intraseasonal (30-100 days) variability of the tropical climate, and has strong societal impacts at an almost global scale (Madden and Julian 1972, 1994; Zhang 2005). The Madden-Julian oscillation has a strong seasonality and its central latitude follows roughly the movements of the Inter-Tropical Convergence Zone (ITCZ; Zhang and Dong 2004). The MJO can be very broadly defined as eastward-propagating perturbations of the tropical convection in the 30-100 days range. During the MJO active phase, anomalous convection develops over the tropical Indian Ocean and propagates eastward at a slow speed of about 5 m/s into the Pacific Ocean, before fading at the eastern edge of the ITCZ/South Pacific Convergence Zone (SPCZ).

The eastward propagation of the MJO is slow compared to atmospheric moist Kelvin waves (~15-20 m/s, Wheeler and Kiladis 1999), and many mechanisms have been proposed to explain this slow propagation. The most prevalent one seems to be the ―frictional-convective interaction with dynamics”. The Kelvin-Rossby wave structure of the response to heating (Gill 1988) is associated with frictional convergence in the boundary layer to the east of the convective center (Wang 1988), providing a low-level humidity source. This frictional convergence process interacts with CISK (conditional instability of the second kind, Charney and Eliassen 1964) mechanism - that relates low-level convergence (divergence) to atmospheric heating (cooling) – to create a slow eastward propagating mode.

While coupling between convection and dynamics probably holds many keys to the MJO properties, the coupling with the oceanic mixed layer also seems to influence the MJO. The ocean surface layer is the main source of moisture for the atmosphere (5 m of water has the same heat capacity as the entire tropical tropospheric column) and varies significantly with the MJO. MJO-related, surface, latent-heat and short-wave flux variations can exceed +/-

50 W m^{-2} and zonal wind variations can exceed 5 m/s (see reviews of Hendon 2005, Zhang 2005, Waliser 2005). Prior to an MJO active phase, clear-sky and low wind-speed conditions prevail, warming SST through diminished air-sea fluxes and oceanic mixing (e.g. Waliser et al. 1999; Inness and Slingo 2003; Maloney and Sobel 2004). These SST anomalies can in turn favour eastward propagation of MJO convection. The MJO is indeed generally more realistic, with enhanced eastward propagation, in AGCMs coupled to a slab-ocean or Ocean GCM (Zhang et al. 2005; Watterson and Syktus 2007), even if a counter-example exists (Hendon 2000). Coupling can also improve forecasts of the MJO (see review of Waliser 2005, and also Woolnough et al. 2007).

The recent advent of satellite microwave data has highlighted regions of strong SST response to the MJO during austral summer (Harrison and Vecchi 2001; Duvel et al. 2004; Saji et al. 2006; Duvel and Vialard 2007). One of these regions is the thermocline ridge between 5°S and 10°S in the Indian Ocean, also known as Seychelles-Chagos Thermocline Ridge (SCTR, Xie et al. 2002, Yokoi et al. 2008, Hermes and Reason 2008). The climatological wind curl in this region favours a shallow thermocline, and this property maintains a shallow, reactive mixed layer, which might explain the strong SST variability in this region (Duvel and Vialard 2007). The 5°S-10°S band in the Indian Ocean exhibits a strong heat content variability at interannual timescales (Masumoto and Meyers, 1998), which seems to be more directly caused by the Indian Ocean Dipole (IOD, Saji et al. 1999; Webster et al. 1999) than by El Niño / La Niña (Rao and Behera 2005). Duvel et al. (2004) and Vialard et al. (2009) showed that interannual variability of the thermal content along the SCTR could modulate the mixed layer depth, and thus the SST response to the MJO. They also proposed that this SST modulation might feedback onto the atmosphere and modulate the interannual variability of the MJO.

Recent studies have also suggested that the diurnal cycle could also influence the MJO.

A thin (≤ 1 m), warm, mixed layer can develop during the day throughout MJO break phase due to low-wind and clear-sky conditions. Such oceanic layer can strongly enhance SST diurnal peak and amplitude (by about 1° to 2°C), and daily mean (by about 0.2°-0.5°C) (e.g. Bernie et al. 2005). Diurnal warm layers often have broad horizontal extents (larger than ~500-1000 km). They appear in already warm regions (mean SST > 28°C), which are very sensitive to small SST changes because of the non-linearity of the Clausius-Clapeyron equation. They favour diurnal convection by increasing evaporation, warming and destabilizing the low-level atmosphere (Kawai and Wada 2007; Yasunaga et al. 2008), and help to moisten the lower troposphere gradually during the MJO break phase, creating favourable conditions for deep convection and MJO onset (Godfrey et al. 1998). So they possibly play an essential role in onset, amplitude, propagation and/or termination of the MJO (e.g. Bernie et al. 2007, 2008; review of Kawai and Wada 2007). A recent study even showed that taking the diurnal cycle into account could improve forecasts of the MJO (Woolnough et al. 2007).

Early descriptions of the MJO coined it as the “30-60 day oscillation” (e.g. Madden and Julian, 1994). The MJO period band is in fact broader during boreal winter (~30-100 days) compared to boreal summer (~30-50 days) (e.g. Zhang and Dong 2004). Saji et al. (2006) pointed out that the timescale of convective variability was longer around 8°S than at the equator in the eastern Indian Ocean, and suggested that there might be two types of intraseasonal variability in the Indian Ocean (a 30-50 day mode in the equatorial band and a lower frequency mode further south). They also showed that the SST response to the southern mode was larger, possibly because of longer periods (Duvel and Vialard 2007).

In this paper, we investigate in more detail the differences in timescales and properties of the austral-summer MJOs along the equator and in the 5°-10°S band. We first analyze how different the oceanic and atmospheric anomalies related to MJO are in both cases, distinguishing precisely the two MJO types[1]. We then investigate how both types of MJO variability are influenced by interannual variability, notably in the SCTR region as suggested in several earlier studies (e.g., Duvel et al., 2004; Saji et al., 2006: Duvel and Vialard, 2007; Vialard et al. 2008, 2009). Section 2 presents the data and analysis methods we used. In section 3, we analyze the observed oceanic and atmospheric anomalies related to the two MJO types. The higher-frequency MJO (HF-MJO, 35-50 days) tends to be symmetric with respect to the equator, while the lower frequency MJO (LF-MJO, 55-100 days) is maximum around 8°S. The LF-MJO is associated with stronger SST, SST diurnal cycle and upper–ocean, heat-content signatures. Section 4 investigates interannual variations of the two MJO types, and shows that the lower-frequency type has larger amplitude following negative IOD years. Section 5 then provides a summary and suggests mechanisms that could explain the difference in properties between the two MJO types. These hypotheses will be tested through a set of coupled general circulation model (CGCM) in a sequel to this study.

2. Data and methods

2.1 Observations

Outgoing Longwave Radiation (OLR) is a classical proxy for deep convection in the tropics and widely used to characterize the MJO. We use the daily 2.5°×2.5° interpolated product from (Liebmann and Smith 1996) available from 1974 to 2008 with a gap in 1978.

The Tropical Rainfall Measuring Mission Microwave Imager (TMI) (3-day mean every day, 1998-2007; Wentz et al. 2000) is used to investigate SST intraseasonal variability,

[1] We prefer to use the term ―type" rather than ―mode", as the broad properties (eastward propagation in the 30-100 day band) and main mechanim (coupling between atmospheric dynamics and convection) are likely the same for the two MJO types, even if ocean-atmosphere interactions could also play an important role for the low-frequency MJO type.

whereas NOAA Optimum Interpolation SST V2 data (for 1981-2007, Reynolds et al. 2002) and Extended Reconstructed SST (ERSST V2 for 1974-1981; Smith and Reynolds 2004) are used to study interannual timescales. Afternoon and night SST from the Advanced Very High Resolution Radiometer (4 km AVHRR Pathfinder Version 5.0) are used to estimate the variations in amplitude of SST diurnal cycle for 1985-2002, and also in daily mean SST for 1985-2007. As AVHRR SST is sensitive to cloud cover, we kept only data with a quality flag higher or equal to 4 (on a range from 1 to 7). We also pay particular attention on drifts in passing local time during the day (Stuart-Menteth et al. 2003) and excluded periods when day-pass is too late. Note that our AVHRR-based estimate of SST diurnal amplitude is weaker than TMI measurements (available on a shorter period) by about a factor of 2 (Kawai and Wada 2007). With two passes per day, it cannot provide a precise estimate of the absolute SST diurnal amplitude, but it can help to assess the variability of SST diurnal amplitude.

To assess observed wind variability on the longest period possible, we merged data from daily Quick Scatterometer (QUIKSCAT, 1999-2007, http://www.ssmi.com/qscat/), weekly European Remote Sensing (ERS) scatterometers winds (from April 1992, http://www.ifremer.fr/cersat, Bentamy et al. 1996) and daily Special Sensor Microwave / Imager (SSMI) wind speed (from 1987, Goodberlet et al. 1989), the later being combined with ECMWF reanalysis wind direction [Atlas et al. 1996].

Ocean heat content and thermocline depth variations are investigated using sea level anomaly (SLA) from TOPEX/Poseidon and JASON satellites (AVISO product). We also use mixed layer depth estimates form oceanic reanalyzes produced by the CERFACS within the ENSEMBLES project (Weaver et al. 2005; Daget et al. 2008).

All satellite data are regridded on a 1°x1° grid, except for OLR, and averaged on pentads. For each dataset, the pentad seasonal cycle, calculated over the longest available period, is removed to obtain interannual anomalies.

2.2 Methods

In this paper, we use a space-time spectral analysis similar to that of previous studies (Takayabu 1994; Wheeler and Kiladis 1999) to evaluate the timescales of the eastward propagating components of the convection and its latitudinal distribution.

We will use a lag-composite analysis to extract the two intraseasonal types of convective variability. For that, we use the 90°E, 10°S-10°N average, OLR anomaly during DJFM as an index of convective activity. This index will be band-pass filtered in three frequency bands (justification later in the text): 30-120 days, 35-50 days and 55-100 days, so as to obtain filtered indices of MJO for these timescales ($OLR_{filt\,90°E}$). (Note that as a Lanczos filter is used with a 1 year moving window, the resulting band-pass filtered signal in DJFM will actually contain some information related to signals in an extended boreal winter season, larger by about half of the MJO period (i.e. about one month) on each side of DJFM (i.e. ~NDJFMA).) This index can be used to make weighted composites for the active (filtered OLR < 0) phases of the MJO, where the weight is the filtered index when negative at day 0, so $OLR_{filt\,90°E} \times H(-OLR_{filt\,90°E})$ where *H(x)* denotes the Heavyside function (*H*=0 if *x*<0, *H*=1 if *x*>0). The weighted composite (*wcompos*) of a field *Y* (e.g. SST, wind, OLR, possibly lagged with $OLR_{filt\,90°E}$ to obtain lag-composites) is computed using the formulae:

$$wcompos(Y) = \frac{\int Y \times OLR_{filt\,90°E} \times H(-OLR_{filt\,90°E})dt}{\int OLR_{filt\,90°E} \times H(-OLR_{filt\,90°E})dt}$$

These weighted composites are quite similar to a linear regression for only negative values of the MJO index $OLR_{filt\,90°E}$, giving similar results to simple composites but with more statistical information. The interest of weighted composites compared to standard linear regression is that the active and break phases of the MJO can be clearly separated, so that the MJO phase captured by the statistical method is well known. Note that the composite analyses presented here were also done with linear regressions and give rather similar results. The fields to be composited on MJO index are band-pass filtered in the 30-120 days band, except if noted. Weighted composites are computed on the MJO index of December to March (DJFM) period.

In section 4 on MJO interannual variations, the weighted composites have also been computed using the MJO index of Wheeler and Hendon (2004). The negative values of their RMM2 index correspond to an active phase of the MJO over the eastern Indian Ocean, similar to the MJO index previously defined. As this index is not filtered temporally, it can be helpful to test the possible sensitivity of the results in section 4 to the temporal filter used. Similar results were obtained for the interannual variations of MJO composites when using the RMM2 index or the 30-120 days MJO index. For clarity, only the results with the MJO index $OLR_{filt\,90°E}$ will be presented here.

Statistical significances of correlations, regression coefficients and composites are calculated using the Student's t-test, taking into account effective degrees of freedom for MJO composites (and their decrease when doing composites for only positive or negative IOD years).

In this paper, we will examine the influence of El Niño Southern Oscillation (ENSO) and Indian Ocean Dipole (IOD) on MJO variability over the Indian Ocean. We will use the classical Niño3.4 (120°W to 170°W, 5°N to 5°S) index in DJF for ENSO. For the IOD, we use a new index in addition to the conventional dipole mode index (DMI, Saji et al. 1999). Our index is based on OLR and is defined as the southeast (80°E-100°E; 10°S-5°S) minus southwest (50°E-70°E; 5°S-0°) OLR poles in SON. This OLR IOD index (OLR IOD) has three advantages. First, OLR, a robust proxy of atmospheric deep convection and heating rate in the tropics, is less subject to errors than long-term SST measurements (which rely heavily on surface infra-red emission and are subject to masking by clouds; Wentz 2000). Second it is available from 1974 onward whereas SST satellite observation starts in 1985. Third, this index based on convection is dynamically linked to the winds that force SCTR thermocline variability. During SON, this OLR index is very well correlated with the conventional SST DMI (0.92) and moderately with Niño3.4 SST (corr. 0.54, signif. 99.5%). Our index is thus well representative of the IOD, which is somewhat influenced by ENSO. Based on a threshold of 50% of the standard deviation, there are 14 negative and 8 positive years over the 1974-2008 period. Tests using other threshold values, or the DMI index instead of our OLR index, give qualitatively similar results.

3. Characteristics of the two austral-summer MJO types

Figure 1 shows spectra of OLR and SST for austral summer in the eastern Indian Ocean. As suggested by (Saji et al., 2006), the strongest peak of convective variability is observed at longer periods (55-80 day) near 8°S, while the secondary peak is at shorter periods (35-45 days) and located at the equator. The SST response is also much larger at 8°S. Figure 2a shows a zonal wavenumber-time OLR spectrum zoomed on timescales corresponding to the MJO. Based on this analysis, we computed the latitudinal dependence of the eastward propagating part of the OLR signal (with speed between 2.5 m/s and 15 m/s, see continuous lines on Fig. 2a) over the whole globe (Fig. 2b) and Indian Ocean (Fig. 2c). At global scale, the most energetic eastward propagating convective signal during Austral summer is found south of the equator, between 4°S and 12°S with a period of roughly 55 to 90 days. Over the Indian Ocean, this signal is still the main pattern but a secondary maximum is now emerging around the Equator with a period around 35-45 days.

In order to diagnose the spatial properties of the signals at those two timescales, and determine if they are two different types of variability, we will use band-pass filtering. Even if

MJO consists of episodic pulse events (Zhang 2005), this standard technique permits to capture in a simple way the amplitude of MJO events separated by a characteristic period.

We have selected two period bands: 35-50 days and 55-100 days bands. The choice of these bands has been determined by three constraints: they (1) are centered approximately on the peaks seen in Figs. 1 and 2c, (2) have the same frequency width and (3) do not overlap. Hereafter in the text, we will use the name high/low frequency (HF/LF-MJO) to designate the different types of MJO variability associated with these two frequency bands. We will further use the abbreviations LF and HF to design the 55-100 and 35-50 days band, respectively. Figure 3 shows the spatial distribution of the OLR and SST variability in those two frequency bands. In agreement with figure 2, figures 3b,d suggest that HF OLR variability is equatorially confined over the Indian Ocean and shifts southward only over the maritime continent and western Pacific. On the other hand, the stronger LF OLR variability is clearly localized between 5°S and 15°S, both in the onset region (the Indian Ocean) and further east.

HF and LF SST variability (Figs 3 a,c) shows similar patterns but the amplitude of LF SST standard deviation is significantly stronger. The LF-MJO is associated with stronger OLR and wind perturbations over the SCTR and the region between Australia and Indonesia, which are characterized by a shallow and responsive mixed layer (Harrison and Vecchi, 2001, Duvel et al., 2004; Bellenger and Duvel 2007; Vialard et al., 2008, 2009). This shallowing explains probably the larger SST response there for the LF-MJO. In addition, amplitude of the SST response is also expected to grow with the timescale of forcing (Duvel and Vialard, 2007), and is thus expected to be larger for the LF-MJO type.

Figures 4 and 5 show weighted composites of SST and its diurnal amplitude (Fig. 4), OLR (Fig. 5) and surface wind, for the HF and LF-MJO. These figures illustrate the MJO patterns during the onset of convection over the Indian Ocean (1st and 2nd columns) and later during its propagation toward the maritime continent (3rd and 4th columns). In the Indian

Ocean, the HF-MJO convection onset is mostly located along the equator, whereas the LF signal appears over the SCTR and maintains maximum values between 5°S and 10°S during its eastward propagation (Fig. 5). For both types, the lead-lag relation between OLR and SST is similar to previous studies (see review of Waliser 2005); warm SST anomalies follow/lead MJO inactive/active phase by about a quarter of period. However, the oceanic response related to the LF type is much stronger than that related to HF type, with warm SST anomalies exceeding 0.2°C over a large domain and important anomalies of SST diurnal amplitude over the southern Indian Ocean (1st and 2nd columns in Fig. 4).

Farther east, the oceanic signature of MJO propagation is also different for the two timescales (3rd and 4th columns in Fig. 4). Within the maritime continent, warmer SST with a larger diurnal cycle is observed for the LF-MJO component before the passage of MJO active phase. Interestingly, convection (as well as precipitation, not shown) anomalies over north Australia are significantly stronger for the LF-MJO, suggesting that this LF type has a greater impact on North Australian weather than the HF one.

4. Interannual variations of the austral-summer MJO types

Previous studies (e.g. Harrison and Vecchi 2001, Duvel et al. 2004, Saji et al. 2006, Duvel and Vialard 2007, Vialard et al 2008, 2009) have suggested that interannual variability of the oceanic stratification could modulate the SST signature of the MJO and even maybe the MJO itself. In this section, we will investigate the LF and HF-MJO types interannual variability. The interannual variations of the activity of each of the two MJO types in austral summer (not shown) are not correlated (correlation 0.06), which is an indication that the two MJO types tend to occur independently from one another.

4.1 Interannual modulation of LF-MJO activity

To understand what can modulate LF-MJO, Figure 6 shows interannual surface atmospheric and oceanic anomalies during the boreal winter (DJFM in Figs 6c,d) and the preceding fall (SON in Figs 6a,b) regressed on the amplitude of the LFMJO activity during the boreal winter. The clearest signal for the regressed variables in DJFM is in the sea-level anomaly (SLA, Fig. 6c), with negatives values in the SCTR associated with an intensification of the LF type. Similar results are obtained over a longer period when using SLA from various oceanic re-analysis products. The same analysis for SST, OLR and surface wind in boreal winter show small amplitude signals in the Indian Ocean, and do not seem to be strongly associated with LF-MJO interannual variability (not shown). Other papers (e.g. Vecchi and Harrison, 2001; Duvel et al. 2004) had already proposed that thermocline changes in the SCTR could increase or diminish the amplitude of the SST signature associated with the MJO. Observed interannual variations of the DJFM intraseasonal SST variability in 60°E-90°E, 8°S-3°S are indeed anti-correlated (-0.60, significant at the 99% confidence level) with mean DJFM SLA along the thermocline ridge. The present paper shows that, in addition, the amplitude of the LF-MJO type itself varies interannually with the amplitude of LF SST variability (see fig. 6d and first column of Table 1) and with the thermocline depth variability in the SCTR region (Fig. 6c).

The origin of the sea-level anomaly seen in figure 6c can easily be traced back to ocean-atmosphere conditions in preceding September-November (SON). The wind, SST and OLR pattern in SON is consistent with a negative phase of the IOD. Negative IOD are known to force off-equatorial Rossby upwelling waves propagating slowly toward the south-west Indian Ocean and generating the negative sea-level anomaly seen in Fig. 6c (Masumoto and Meyers, 1998; Xie et al., 2002; Rao and Behera, 2005; Vialard et al., 2009). Figures 6a and 6b show that negative IOD tend to occur during fall (SON) that precede winters with strong LF-MJO activity. There tends to be a phase locking of IOD events to El Niño events (Gualdi et al. 2003, Yamagata et al. 2004). Hence, maps similar to figure 6a,b,c show a typical La Niña pattern in the Pacific Ocean (not shown). To isolate which of the IOD or ENSO does mostly influence the LF-MJO type, partial correlations for different pairs were computed (Table 1). Even if the LF-MJO is correlated with Niño3.4 SST, it is IOD variability (see definition of the index in section 2) rather than ENSO that explains most of the variance of the southern low-frequency MJO.

4.2 Impact of IOD on HF-MJO and LF-MJO

In the rest of the section, we will assess systematically the impact of IOD on the LF and HF MJO types. To that end, we will use the IOD index described in section 2. We first perform analyses similar to Figs. 1, 2 and 4 separately for positive and negative IOD years.

4.2.1 Modulation of SST and OLR intraseasonal variability by IOD

Fig. 7 shows the changes in SST and OLR spectrum after a negative or positive IOD year. At the equator, the SST spectrum is not significantly changed. On the other hand, there is a clear increase of OLR equatorial variability at lower frequencies after negative IOD years. At 8°S, there is an increase of intraseasonal SST variability in the SCTR following negative IODs. This again confirms what was hypothesized by several previous studies (e.g. Vecchi and Harrison, 2001; Duvel et al. 2004): a thinner SCTR thermocline favours a local increase of SST intraseasonal variability (cf. their significant correlation of 0.60 shown previously in section 4.1). Second, there is also an increase in OLR LF variability following a negative IOD (Figure 7b). This increase is almost within the range of uncertainty, but fig. 6a,b shows that the negative relationship between LF-MJO, estimated with the simpler method using band-pass filtering, and IOD is significant.

4.2.2 Latitudinal-frequency distribution modulated by IOD

Figure 8 (similar to Fig. 2 but after positive/negative IOD years) shows changes in the eastward-propagating components of OLR. Over the globe (left and middle panels), the OLR eastward-propagating signal is stronger after negative IOD years, with a maximum at LF (Fig. 8d). In the Indian Ocean, the differences are the strongest with a clear unique peak at LF centered on 8°S after negative IOD years. After positive IOD years, there are two spectral peaks. The 8°S LF peak remains, but is weaker than after negative IOD years. But another peak at HF appears at the equator. The ―HF-MJO type" is much better defined after positive IOD years and quasi-inexistent after negative IOD years.

4.2.3 spatial patterns of MJO composites

Figure 9 (cf. figures 4 and 5) shows the changes in the HF and LF types following a positive or negative IOD. The MJO index used to produce figs 9 and 10 is the 30-120 days one, so that MJO period is not constrained *a priori*. Hence the difference in latitude and period respectively obtained eventually in Figs 9 and 10 can thus only originate from the different intrinsic periods of MJO events after positive and negative IOD. After positive IOD years, an equatorial MJO onset with symmetric patterns similar to the HF-MJO type described in section 3 seems to be favoured. On the other hand, after negative IOD years (and also to some extent after neutral IOD conditions, not shown), the patterns are similar to those of the LF-MJO southern type: stronger SST signature with enhanced warming (cooling) during MJO break (active) phase, stronger diurnal cycle signal and maximum wind and OLR anomaly shifted to the south.

4.2.4 Propagation: extent and speed

Figure 10 finally illustrates the impact of IOD (and ENSO) on the propagation characteristics of the MJO. Time-longitude (15°S-5°N) diagrams of lagged weighted composites are plotted for positive/negative IOD. The MJO OLR signal is stronger and propagates further eastward (to the date line) after negative IOD events than after positive ones. The difference in MJO timescales shown previously through spectral analyses (Figs. 7 and 8) is also evident in Fig. 10, especially in the Indian Ocean, with a shorter/longer

(~30/60) days period between two successive non-active phases after positive/negative IOD (due to the “pulse” nature of the MJO convective event (e.g. Zhang, 2005), these periods should be somewhat shorter than the ones between two active phases). So as to better differenciate the southern LF-MJO, stronger after negative IOD, from the equatorial HF-MJO, stronger after positive IOD, Hovmullers with thinner latitudinal widths of 5° were computed. Slower propagation speeds in the ITCZ/SPCZ are observed for the southern (12°S-7°S) MJO after negative IOD (~4.5m/s) compared to the equatorial MJO (2.5°S-2.5°N) after positive IOD (~6.5 m/s), for the active as well as for the non-active phases (not shown). MJO event after negative IOD tends to be to the south and to have asymmetric circulation anomalies. The asymmetry weakens low-level frictional convergence/divergence processes and could be at the origin of MJO slowdown [Salby et al. 1994]. This issue requires further studies. To conclude this time-longitude analysis, the longer longitudinal pathway in the ITCZ/SPCZ (and slower speed) of MJO events after negative IOD could possibly explain the increase in MJO period.

This section has shown a strong relationship between Indo-Pacific interannual anomalies of the ocean-atmosphere system during the boreal fall of a particular year and characteristics of the MJO during the following winter. We have been able to separate the two MJO types without any help of temporal filter, in contrast to Section 3. This separation suggests that the two MJO types evidenced here are not the result of an artifact related to the filtering method and that they represent two physically distinct MJO types. It also suggests that the southern LF and equatorial HF MJO types do not simply correspond to the MJO in austral summer and equinoxial seasons respectively.

5. Summary and Discussion

In this final section, we will first summarize the results of this paper, then propose two main hypotheses for the processes explaining the interannual variations of the LF/HF-MJO types, and finally discuss physical mechanisms possibly involved in the LF-MJO type.

5.1 Summary

In the present paper, we have used observations to describe oceanic and atmospheric signals associated with the Madden-Julian oscillation in austral summer. The MJO can be broadly defined as eastward–propagating, convective signals in the 30-100 days range. The current analysis suggests that there are in fact two separate spectral peaks within the 35-50 days and 55-100 days band, with different properties, which we named the high-frequency (HF) and low-frequency (LF) austral-summer MJOs. The LF-MJO is maximum under the ITCZ, at around 8°S and has a clear oceanic signature, in both SST and amplitude of the SST diurnal cycle. The HF-MJO is centered on the equator, and has a significantly weaker oceanic signature, despite roughly equivalent amplitudes of the atmospheric perturbations. These two MJO types have a clear interannual amplitude variability that can be related to the IOD (and concurrent ENSO). The LF-MJO and the index that we use in this study are more directly related to the IOD than to ENSO (Table 1), suggesting that the IOD has the largest influence. After a negative IOD, the HF-MJO type is almost non-existent (whereas it is rather strong after a positive IOD). On the other hand, the LF-MJO type shows increased variability in both atmospheric convection and oceanic responses after a negative IOD, with a propagation extending further east, having potentially a stronger impact on Australian and south-west Pacific weather variability. In the following subsection, we will propose two main hypotheses that could explain some of the observed statistics that we presented in this paper.

5.2 Discussion on interannual variations: physical hypotheses

5.2.1 Importance of the background state

The first and most straightforward physical hypothesis is that the mean state of the atmosphere is directly influencing the properties of the MJO type that can develop. Figure 11 shows some variables illustrating the state of the ocean-atmosphere system in DJFM after positive and negative IOD events, which characterize the two different states over which MJOs develop. This figure shows patterns both characteristic of the IOD and ENSO (they tend to co-occur, although not systematically). The changes in mean state could explain some of the results of this study. For example, the low-level westerlies and convection / rainfall from south-eastern Indian Ocean to western Pacific are stronger after a negative IOD than after a positive one (Fig. 11a), and both provide a favourable ground for MJO propagation (Inness and Slingo 2003; Zhang and Dong 2004; Watterson and Syktus 2007). Furthermore, as negative IOD seem to favour a southward MJO onset and propagation, this southern shift could allow the MJO to be less perturbed by the lands of the maritime continent, and to propagate further east. All these processes could explain why, after negative IOD, MJO tends to be globally stronger and to propagate more to the south and further east in a more active SPCZ, having hence a longer (and slower) pathway. The latter could in turn explain the longer period/lower frequency tendency of the MJO after negative IOD events (rather than the contrary). Also, the equatorial HF-MJO type might be an expression of interaction between linear equatorial atmospheric dynamics and convection, and as such be favoured during years when there is convection along the equator in the Indian Ocean, i.e. more after positive IOD. On the other hand, when considering the atmospheric background properties over the SCTR region after a negative IOD, the observed significant changes cannot explain why the MJO tends to onset over the SCTR: westerlies are weaker (figures 11af), convection is decreased (figures 11bg) and the surface is colder (figures 11ch) over the SCTR after a negative IOD.

The processes of how the atmospheric background state might be responsible for the increased LF-MJO remain to be investigated against existing MJO theories.

5.2.2 Importance of ocean-atmosphere coupling

The other possibility is that, as suggested by many studies, coupling with the ocean is important for the properties of the MJO, for its onset and for its eastward propagation (e.g. Waliser et al. 1999; Inness and Slingo 2003; Maloney and Sobel 2004; Zhang et al. 2005). Some studies also proposed (e.g. Woolnough et al., 2007) that a good description of the diurnal cycle modulation associated with the MJO is needed to improve MJO description and forecasts.

Here, larger intraseasonal SST responses are observed for the LF-MJO type, suggesting that coupling could play a stronger role for LF-MJO than for HF-MJO. We have shown, as suggested by other previous studies (e.g. Duvel et al. 2004), that the SST response to the MJO was stronger after negative IOD events. This increased sensitivity has been explained by previous studies: a negative IOD forces upwelling Rossby waves in the 5°-10°S band in the eastern and central Indian Ocean, which later raise the thermocline in the SCTR region. This raised thermocline modulates the mixed layer depth and hence the reactivity of the SST to air-sea fluxes (Duvel et al. 2004), but also the amount of entrainment / upwelling into the mixed layer (Lloyd and Vecchi, 2009; Vinayachandran and Saji, 2008; Resplandy et al., 2009), resulting in stronger SST response to the LF-MJO after a negative IOD in the SCTR, which is also the breeding ground for MJO onset.

Extending these results, we also show here that the amplitude of the LF-MJO itself is increased following negative IOD years, (and is significantly correlated to increased amplitude of LF SST variability over the SCTR). While this LF-MJO increase could be explained by changes of the atmospheric mean state, and could explain the increased LF SST variability, the other alternative is that the larger oceanic response after the negative IOD years in the SCTR favours larger amplitude of the southern LF-MJO, as suggested by Duvel et al. (2004). We also observe here that the MJO modulation of the diurnal cycle seemed stronger[2], possibly partly because the reduced mean westerlies and cloud cover after IOD could favour the occurrence of diurnal warm layers. This enhancement of SST diurnal cycle modulation by the MJO could also enhance SST intraseasonal variability and air-sea coupling in this region, hence favouring the southern MJO onset at the end of negative IOD events. To summarize, these two processes - thinner MLD and increased SST diurnal cycle - can promote local MJO onset along the SCTR (even if the mean DJFM ITCZ is weaker and mean SST is colder in the region).

However, how air-sea coupling might modify the properties of the LF-MJO downstream of the SCTR region is unclear. The region between Australia and Indonesia has large SST intraseasonal variability (e.g. Duvel and Vialard 2007) and a shallow MLD (Bellenger and Duvel 2007). But the interannual modulation of the SST intraseasonal variability in this region has not been studied. In the western Pacific, the SST intraseasonal variability in response to the MJO is much smaller (Duvel and Vialard 2007), and the thermocline is deep, providing no obvious mechanism of control of the SST intraseasonal variability by lower frequencies. Whether interannual modulation of air-sea coupling in the SCTR region is enough to modify the properties of the MJO downstream to the western Pacific thus remains to be investigated more thoroughly.

5.2.3 Further steps

It is quite difficult to assess from observations only the relative importance of the processes mentioned above (i.e. atmospheric background and/or ocean-atmosphere coupling) in setting the properties of the HF and LF austral summer MJO types. On the other hand,

[2] The composites being however rather noisy because of observational uncertainties, this study suggests the need for further studies, when more accurate long-term observations will be available

these hypotheses could be tested in general circulation models with the observational analyses proposed here as a benchmark. In a follow-on study, we will partly follow that objective, using a coupled general circulation model, which is able to resolve the SST diurnal cycle.

To conclude, the present study highlights important scale interactions and emphasizes the necessity to implement ocean-atmosphere observing/modeling systems for the entire tropical Indian Ocean, including its southern part, with sufficient vertical and temporal resolution. The ability to predict the MJO and its global impacts will depend not only on the knowledge of large-scale conditions, but also on an accurate estimate of the Indian Ocean variability on a regional scale.

Acknowledgments. The authors would like to thank JAMSTEC, especially FRCGC and the Earth Simulator Center, for their great hospitality and the high performance material and computer facilities they offer. Dr. Sophie Cravatte, Dr. Fabien Durand, and all the LEGOS and LOCEAN teams are greatly thanked for their support of this research project. Most of the observations data were made available mainly by NOAA/NCEP/CPC through Climate Diagnostics Center (CDC), IRI/LDEO Climate Data Library and AVISO servers. AVHRR Pathfinder SST is NODC/NOAA. QuikScat data are produced by Remote Sensing Systems and sponsored by the NASA Ocean Vector Winds Science Team. Those data were obtained from the IFREMER (CERSAT) ftp server. The authors also wish to acknowledge the use of NOAA/PMEL Ferret program for analysis and graphics in this paper. The Japan Society for the Promotion of Science (JSPS) and the French Research Agency (ANR, Project INLOES) funded this work.

REFERENCES

Atlas R., R. N. Hoffman, S. C. Bloom, J. C. Jusem, and J. Ardizzone, 1996: A Multiyear Global Surface Wind Velocity Dataset Using SSM/I Wind Observations. *Bull. Amer. Meteor. Soc.,* 77, 869-882.

Bellenger, H. and J.P. Duvel, 2007: Intraseasonal Convective Perturbations related to the Seasonal March of the Indo-Pacific Monsoons, *Journal of Climate*, 20, 2853-2863.

Bentamy A., Y. Quilfen, F. Gohin, N. Grima, M. Lenaour and J. Servain, 1996: Determination and validation of average wind fields from ERS-1 scatterometer measurements. *The Global Atmosphere and Ocean System*, **4**, 1-29.

Bernie, D. J., S. J. Woolnough, J. M. Slingo and E. Guilyardi, 2005: Modeling of diurnal and intraseasonal variability of the ocean mixed layer. *J. Climate*, 18, 1190–1202.

Bernie D.J., Guilyardi E., Madec G., Woolnough S.J., Slingo J.M., 2007: Impact of resolving the diurnal cycle in an ocean-atmosphere GCM. Part 1: Diurnally forced OGCM. *Clim Dyn* 29:575–590.

Bernie, D. J.; Guilyardi, E.; Madec, G.; Slingo, J. M.; Woolnough, S. J.; Cole, J., 2008: Impact of resolving the diurnal cycle in an ocean atmosphere GCM. Part 2: A diurnally coupled CGCM. *Climate Dynamics*, 31, 909-925.

Charney, J. G., and A. Eliassen, 1964: On the growth of the hurricane depression. *J. Atmos. Sci.*, **21,** 68–75.

Daget, N., Weaver, A. T. and M. A. Balmaseda, 2008: An ensemble three-dimensional variational data assimilation system for the global ocean: sensitivity to the observation- and background-error formulation. *ECMWF Tech. Memo*. No. 562.

Duvel, J. P., and J. Vialard, 2007: Indo-Pacific sea surface temperature perturbations associated with intraseasonal oscillations of the tropical convection, *J. Climate*, **20**, 3056-3082.

Duvel, J.P., R. Roca and J. Vialard, 2004: Ocean mixed layer temperature variations induced by intraseasonal convective perturbations over the Indian Ocean. *J. Atm. Sciences,* **61,** 1004-1023.

Gill, A. E., 1980: Some simple solutions for heat-induced tropical circulation. *Q. J. R. Meteorol. Soc.* **106**, 447–462.

Godfrey, J. S., R. A. Houze, Jr., R. H. Johnson, R. Lukas, J.-L. Redelsperger, A. Sumi, and R. Weller, 1998: Coupled Ocean-Atmosphere Response Experiment (COARE): An interim report. *J. Geophys. Res*., 103, 14,395-14,450.

Goodberlet, M.A., C.T. Swift, and J.C. Wilkerson, 1989: Remote Sensing of Ocean Surface Winds with the Special Sensor Microwave Imager. J. Geophys. Res., 94, 14544-14555.

Harrison, D. E., and G.A. Vecchi, 2001: January 1999 Indian Ocean cooling event. *Geophys. Res. Lett.,* **28,** 3717–3720.

Hendon, H. H., 2000: Impact of air-sea coupling on the Madden-Julian Oscillation in a general circulation model. *J. Atmos. Sci*., **57**, 3939- 3952.

Hendon H. H., 2005: Air-sea interaction, in *Intraseasonal variability of the Ocean Atmosphere Climate System,* edited by W.K.M. Lau and D.E. Waliser, Springer, Heidelberg, Germany.

Hermes, J.C. and C.J.C. Reason, 2008: Annual cycle of the South Indian Ocean (Seychelles-Chagos) thermocline ridge in a regional ocean model, *J. Geophys. Res.,* **113,** C04035, doi:10.1029/2007JC004363.

Inness, P. M., and J. M. Slingo 2003: Simulation of the Madden-Julian Oscillation in a coupled general circulation model. Part I: Comparisons with observations and an atmosphere-only GCM, *J. Clim*., 16, 345–364.

Kanamitsu, M., Ebisuzaki, W., Woollen, J., Yang, S.-K., Hnilo, J. J., Fiorino, M., and Potter, G. L., 2002: NCEP-DOE AMIP-II reanalysis. *Bull. Amer. Meteor. Soc.,* 1631-1643.

Kawai Y. and Wada A., 2007: Diurnal sea surface temperature variation and its impact on the atmosphere and ocean: A review. *Journal of Oceanography* 63(5): 721.

Liebmann, B., and C. A. Smith, 1996: Description of a complete (interpolated) outgoing longwave radiation dataset. *Bull. Amer. Meteor. Soc.,* **77,** 1275–1277.

Llyod I.D. and G.A. Vecchi, 2009: Submonthly Indian Ocean cooling events and their relation to large-scale conditions. *J. Geophys. Res*., submitted.

Madden, R. A., and P. R. Julian, 1994: Observations of the 40–50- day tropical oscillation—A review. *Mon. Wea. Rev.,* **122,** 814– 836.

Maloney E.D. and A.H. Sobel 2004: Surface fluxes and ocean coupling in the tropical intraseasonal oscillation. *Journal of Climate,* **17,** 4368-4386.

Masumoto, Y. and G. Meyers, 1998: Forced Rossby waves in the southern tropical Indian Ocean, *J. Geophys. Res. (Oceans),* **103,** 27589-27602.

Matthews, A. J., 2000: Propagating mechanism for the Madden Julian oscillation. Quart. *J. Roy. Met. Soc*., **126,** 2637-2651.

Rao, S.A., and S. K. Behera 2005: Subsurface influence on SST in the tropical Indian Ocean: structure and interannual variability. *Dyn. Atmos. Ocean*. ,39, 103-135.

Resplandy L., J. Vialard, M. Lévy, O. Aumont and Y. Dandonneau 2009 : Seasonal and intraseasonal biogeochemical variability in the thermocline ridge of the Indian Ocean. *J. Geophys. Res.* , submitted.

Reverdin, G., D. Cadet and D. Gutzler, 1986. Interannual displacements of convection and surface circulation over the equatorial Indian Ocean. *Quarterly Journal of the Royal Meteorological Society* **112**, 43–46.

Reynolds, R. W., N. A. Rayner, T.M. Smith, D. C. Stokes and W. Wang, 2002: An improved in situ and satellite SST analysis for climate. *J. Climate,* **15**, 1609-1625.

Saji, N. H., B. N. Goswami, P. N. Vinayachandran and T. Yamagata, 1999: A dipole mode in the tropical Indian Ocean. *Nature,* **401,** 360-363.

Saji, N.H., S.-P. Xie, and C. -Y. Tam, 2006: Satellite observations of intense intraseasonal cooling events in the tropical south Indian Ocean. *Geophys. Res. Lett.*, **33**, L14704, doi: 10.1029/2006GL026525.

Salby, M. L., R. R. Garcia, and H. H. Hendon, 1994: Planetary scale circulations in the presence of climatological and wave induced heating. *J. Atmos. Sci.,* **51,** 2344–2367.

Smith, T. M., and R. W. Reynolds, 2004: Improved extended reconstruction of SST (1854-1997). *J. Clim.,* 17, 2466-2477.

Stuart-Menteth, A. C., I. S. Robinson and P. G. Challenor, 2003: A global study of diurnal warming using satellite derived sea surface temperature. *J. Geophys. Res*., 108(C5), 3155, doi:10.1029/2002JC001534.

Takayabu, Y. N., 1994: Large-scale cloud disturbances associated with equatorial waves. Part I: Spectral features of the cloud disturbances. *J. Meteor. Soc. Japan,* **72,** 433– 448.

Vialard, J., J-P. Duvel, M. McPhaden, P. Bouruet-Aubertot, B. Ward, E. Key, D. Bourras, R. Weller, P. Minnett, A. Weill, C. Cassou, L. Eymard, T. Fristedt, C. Basdevant, Y. Dandoneau, O. Duteil, T. Izumo, C. de Boyer Montégut, S. Masson, F. Marsac, C. Menkes, S. Kennan, 2009, Cirene: Air Sea Interactions in the Seychelles-Chagos thermocline ridge region, *Bull. Am. Met. Soc.,* **in press.**

Vialard, J., G. Foltz, M. McPhaden, J.-P. Duvel, and C. de Boyer Montegut, 2008: Strong Indian Ocean cooling associated with the Madden–Julian Oscillation in late 2007 and early 2008. *Geophys. Res. Lett.,* **35,** L19608, doi:10.1029/2008GL035238.

Vinayachandran, P. N., and N. H. Saji, 2008: Mechanisms of South Indian Ocean intraseasonal cooling. *Geophys. Res. Lett*., 35, L23607, doi:10.1029/2008GL035733.

Waliser, D. E., K. M. Lau, J.-H. Kim, 1999: The influence of coupled Sea Surface Temperatures on the Madden–Julian oscillation: A model perturbation experiment. *J. Atmos. Sci.*, **56**, 333–358.

Waliser, D. E., 2005: Intraseasonal Variability, in *The Asian Monsoon*, edited by B. Wang, p. 844 Springer, Heidelberg, Germany.

Wang, B., 1988: Dynamics of tropical low-frequency waves: An analysis of the moist Kelvin wave, *J. Atmos. Sci.,* 45, 2051–2065.

Watterson I.G., Syktus J., 2007: The influence of air-sea interaction on the Madden-Julian Oscillation: the role of the seasonal mean state. *Climate Dynamics* 28(7-8): 703.

Weaver, A. T., Deltel, C., Machu, E., Ricci, S. and N. Daget, 2005: A multivariate balance operator for variational ocean data assimilation. *Q. J. Roy. Meteorol. Soc*., 131, 3605-3625.

Webster, P. J., A. M. Moore, J. P. Loschnigg, and R. R. Leben, 1999: Coupled oceanic–atmospheric dynamics in the Indian Ocean during 1997–98. *Nature,* **401,** 356–360.

Wentz, F.J., C. Gentemann, D. Smith, and D. Chelton (2000) Satellite Measurements of Sea Surface Temperature Through Clouds. *Science* 288 (5467), 847.

Wheeler, M., and G.N. Kiladis, 1999: Convectively coupled equatorial waves: Analysis of clouds and temperature in the wavenumber-frequency domain. *J. Atmos. Sci.,* 56, 374-399.

Wheeler, M.C., and H.H. Hendon, 2004: An all-season real-time multivariate MJO Index: Development of an index for monitoring and prediction. *Mon. Wea. Rev*., 132, 1917-1932.

Woolnough, S. J., F. Vitart, and M. A. Balmaseda, 2007: The role of the ocean in the Madden-Julian Oscillation: Implications for MJO prediction. *Q. J. R. Meteorol. Soc*., **133**, 622, 117-128.

Xie, S.-P., H. Annamalai, F.A. Schott and J.P. McCreary, 2002: Structure and mechanisms of south Indian climate variability, *J. Climate,* **9,** 840-858.

Yamagata, T., S. K. Behera, J.-J. Luo, S. Masson, M. Jury, and S. A. Rao, 2004: Coupled ocean-atmosphere variability in the tropical Indian Ocean, in Earth Climate: The Ocean-Atmosphere Interaction, *Geophys. Monogr. Ser.,* **147,** edited by C. Wang, S.-P. Xie, and J. A. Carton, pp. 189–212, AGU, Washington, D. C.

Yasunaga K, Fujita M, Ushiyama T, Yoneyama K, Takayabu Y.N. ,Yoshizaki M., 2008: Diurnal Variations in Precipitable Water Observed by Shipborne GPS over the Tropical Indian Ocean. *SOLA* 4: 97.

Yokoi, T., T. Tozuka, and T. Yamagata, 2008: Seasonal variation of the Seychelles Dome. *J. Climate,* **21,** 3740–3754.

Zhang C., Dong M., 2004 Seasonality in the Madden–Julian oscillation. *J Climate* 17:3169–3180.

Zhang, C., 2005: Madden-Julian Oscillation, *Rev. Geophys.,* **43,** RG2003, doi:10.1029/2004RG000158.

Zhang, C, M. Dong, H. H. Hendon, E. D. Maloney, A. Marshall, K. R. Sperber, and W. Wang, 2005: Simulations of the Madden-Julian Oscillation in Four Pairs of Coupled and Uncoupled Global Models. *Climate Dynamics*, DOI: 10.1007/s00382-006-0148-2.

List of Table and Figures

Table 1. First column: correlations of the standard deviation of LF OLR (DJFM, 55ºE-165ºE, 10ºS-0º) with previous SON OLR_IOD, DMI, Niño3.4 SST over 1979-2008, and with the standard deviation of low-freq. SST in DJFM over the SCTR (60ºE-90ºE, 8ºS-3ºS) from TMI (1998-2007)/Reynolds (1985-2007). Second to fourth column: partial correlations for different pairs, evidencing that rather than ENSO, it is OLR_IOD variability (and to a less extent the DMI) that explains most of the variance of the southern low-frequency MJO.

Fig. 1: Spectra (in amplitude) for SST (°C day, left) and OLR (W m^{-2} day, right) along the thermocline ridge (at 8°S; continuous black lines) and along the equator (dashed black lines) in NDJFM in the Indian Ocean (spectral amplitudes averaged over 60°E-90°E). The vertical/horizontal lines on the right panel show the low and high frequency bands selected (55-100 days and 35-50 days). Light blue lines show the intervals confident at the 90% level. To reduce windowing effect, the component of the signal with periods greater than 125 days was removed before computing the spectra.

Fig. 2: (a) OLR spectrum (in amplitude, global, 10°S-5°N mean) ; (b,c) latitudinal distribution of OLR eastward propagating component (global in (b) and Indian Ocean only (55°E-95°E) in (c)) in austral summer (NDJFM). In (a), the x(y)-axis is zonal wave number (period). The dashed line represents the conventional MJO speed (5m/s). In (b,c), the eastward propagating signal has been calculated by averaging spectrum over positive zonal wave numbers between the two continuous diagonal lines shown in (a) (i.e. between 2.5 m/s and 15 m/s speeds). In (b,c), the x(y)-axis is the period (latitude). The vertical/horizontal lines on the right panel show the LF and HF bands. Unit is in W m^{-2} day.

Fig. 3: maps of standard deviations of SST (TMI, left column; °C) and OLR (right column; W m^{-2}) for MJO HF (upper row) and LF (lower row) bands in DJFM.

Fig. 4: difference between the HF (upper row) and LF (lower row) MJO composites, for SST diurnal amplitudes and daily SST, firstly prior to MJO onset in the Indian Ocean (left columns) and secondly prior to MJO propagation over the maritime continent (right columns). The weighted composites are at different lags for a negative intraseasonal OLR at 90°E, 10°N-10°S (location indicated by the black vertical bars) at t=0 in DJFM. SST diurnal amplitude and daily SST are shown about a quarter to eighter period before the OLR composites of figure 5. Surface winds are plotted for significance higher than 85%. Black contours show the 95% significant level.

Fig. 5: similar to figure 4, but for OLR composites only, at various lags.

Fig. 6: ocean and atmosphere background state in boreal fall (SON) and winter (DJFM) regressed on southern LF-MJO activity in DJFM (OLR 55-100days, 55°E-165°E; 10°S-0º). (a): mean SST (°C, 1974-2007) and wind stress (N m^{-2}, 1987-2007) in fall (SON) before strong low-frequency MJO. (b): same as (a) but for OLR (color, W m^{-2}, 1974-2007). (c): for mean SLA in DJFM (cm, AVISO, 1992-2007). (d): for standard deviation of low-frequency SST in DJFM (TMI, 1998-2007). Surface winds are plotted for significance higher than 90%. The 90% significant level is added in black contours. The boxes defining the OLR-IOD index are shown in (b).

Fig. 7: same as Fig. 1, but for boreal winters following negative (black) and positive (red)

IOD in fall.

Fig. 8: longitude-time spectrum (left column), and latitudinal distribution of eastward propagating component globally (middle column) and in the Indian Ocean (right column), for OLR in DJFM, after positive IOD (upper row) and negative IOD (lower row) in SON (similar method to Fig. 2).

Fig. 9: MJO weighted composites in winter after positive (upper row) and negative (lower row) IOD conditions in fall: for SST (2nd column) and OLR (3rd column) intraseasonal anomalies during MJO onset, and for intraseasonal SST just after the passage of MJO active phase (4th column), in DJFM. Surface winds are plotted for significance higher than 85%. The 90% significant level is added in black contours. In the first column, the difference of the t=-20days and t=0 composites for the diurnal amplitude of SST (its total anomaly, no intraseasonal filtering) is plotted to remove the strong interannual signal (cf. fig. 11e,j), as the latter can not be trivially removed otherwise due to missing data constraints. The MJO index used here has been filtered in the broad 30-120days band, so as to let MJO timescale unconstrained *a priori* (see text for details).

Fig. 10: time-longitude diagrams for lag-composites of OLR (color, to show MJO slow propagation in Indo-Pacific ITCZ-SPCZ) and SLP (contour, to evidence the circum-equatorial propagation as faster moist Kelvin waves), following different IOD conditions in fall: positive (upper) and negative (lower). The diagonal line shows the conventional MJO speed (5m/s). Latitudinal averaging is done over 15°S-5°N to capture the average propagation of MJO convection, shifted to the south during boreal winter. The fields composited here have not been high-pass filtered to limit time-aliasing. The MJO index used here is filtered over the

broad 30-120days band, as in Fig. 9.

Fig. 11: Composites of mean DJFM state after positive (left column) and negative (right column) IOD. 1st line: zonal wind stress (SSMI/ERS1-2/Quikscat; N/m^2), 2nd line: precipitation (mm/d, GPCP), 3rd line: SST (°C, ERSST/Reynolds), 4th line: ocean mixed layer (m, from CERFACS-ENSEMBLES ocean reanalysis), 5th line: amplitude of SST diurnal cycle (°C, AVHRR). 7 (14) positive (negative) IOD events were used for the longest time series (1974-2007, SST, OLR and MLD). However, the shortest record (SST diurnal cycle) contains only 3 (7) positive (negative) events.

TABLE and FIGURES

Std dev. of low-freq. OLR (DJFM, southern) correlated with:	Correlations	Partial corr. for OLR.IOD/Niño3.4	Partial corr. for DMI/Niño3.4	Partial corr. for OLR.IOD/DMI
OLR_IOD (SON)	-0.52(99.8%)	-0.42 (influence of Niño3.4 removed)	-	-0.33 (influence of DMI removed)
DMI (SON)	-0.44 (99%)	-	-0.30 (influence of Niño3.4 removed)	-0.11 (influence of OLR.IOD removed)
Niño3.4 SST (SON)	-0.34 (95%)	-0.04 (influence of OLR.IOD removed)	-0.05 (influence of DMI removed)	-
std dev. of low-freq. SST (DJFM, over the SCTR) from TMI/Reynolds	0.84 (99%)/ 0.62 (99.8%)			

Table 1. First column: correlations of the standard deviation of LF OLR (DJFM, 55ºE-165ºE, 10ºS-0º) with previous SON OLR_IOD, DMI, Niño3.4 SST over 1979-2008, and with the standard deviation of low-freq. SST in DJFM over the SCTR (60ºE-90ºE, 8ºS-3ºS) from TMI (1998-2007)/Reynolds (1985-2007). Second to fourth column: partial correlations for different pairs, evidencing that rather than ENSO, it is OLR_IOD variability (and to a less extent the DMI) that explains most of the variance of the southern low-frequency MJO.

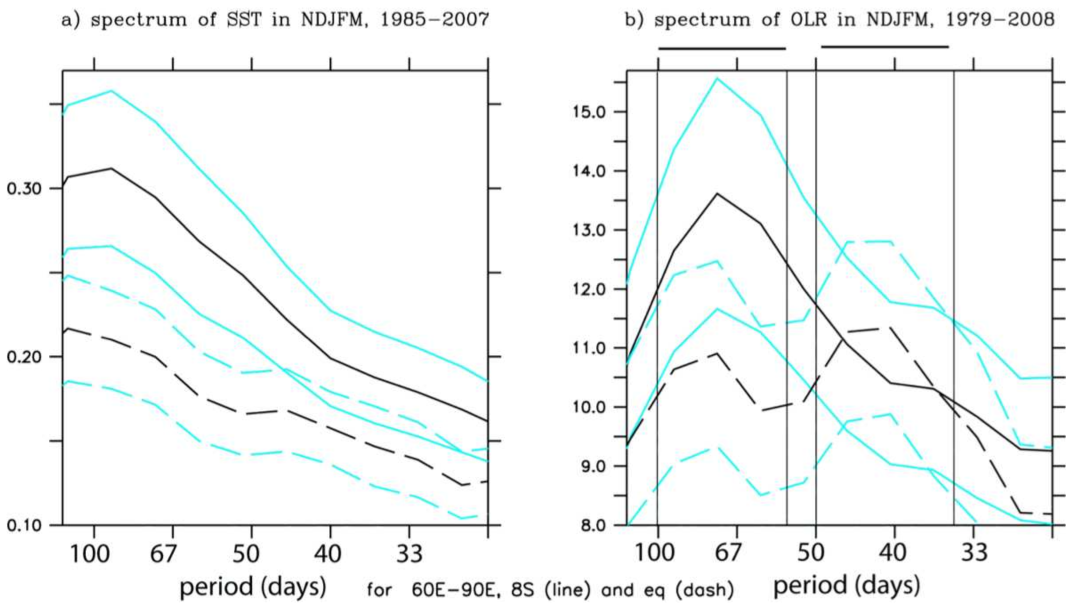

Fig. 1: Spectra (in amplitude) for SST (°C day, left) and OLR (W m^{-2} day, right) along the thermocline ridge (at 8°S; continuous black lines) and along the equator (dashed black lines) in NDJFM in the Indian Ocean (spectral amplitudes averaged over 60°E-90°E). The vertical/horizontal lines on the right panel show the low and high frequency bands selected (55-100 days and 35-50 days). Light blue lines show the intervals confident at the 90% level. To reduce windowing effect, the component of the signal with periods greater than 125 days was removed before computing the spectra.

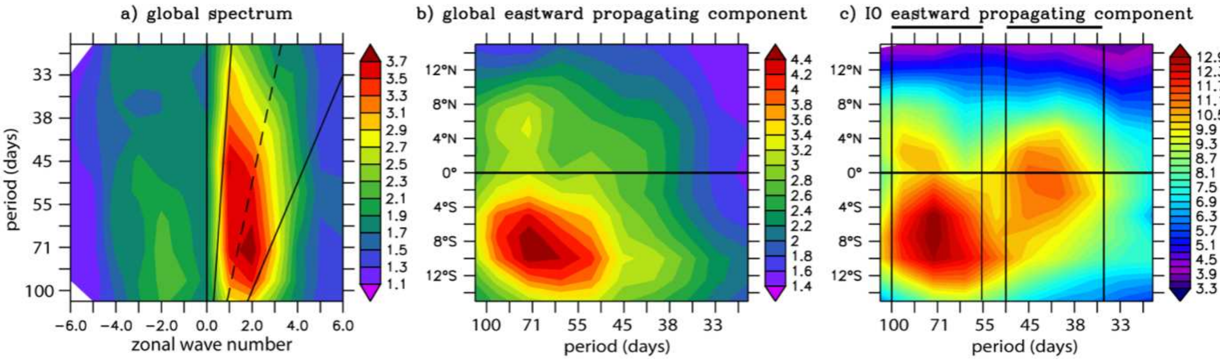

Fig. 2: (a) OLR spectrum (in amplitude, global, 10°S-5°N mean) ; (b,c) latitudinal distribution of OLR eastward propagating component (global in (b) and Indian Ocean only (55°E-95°E) in (c)) in austral summer (NDJFM). In (a), the x(y)-axis is zonal wave number (period). The dashed line represents the conventional MJO speed (5m/s). In (b,c), the eastward propagating signal has been calculated by averaging spectrum over positive zonal wave numbers between the two continuous diagonal lines shown in (a) (i.e. between 2.5 m/s and 15 m/s speeds). In (b,c), the x(y)-axis is the period (latitude). The vertical/horizontal lines on the right panel show the LF and HF bands. Unit is in W m^{-2} day.

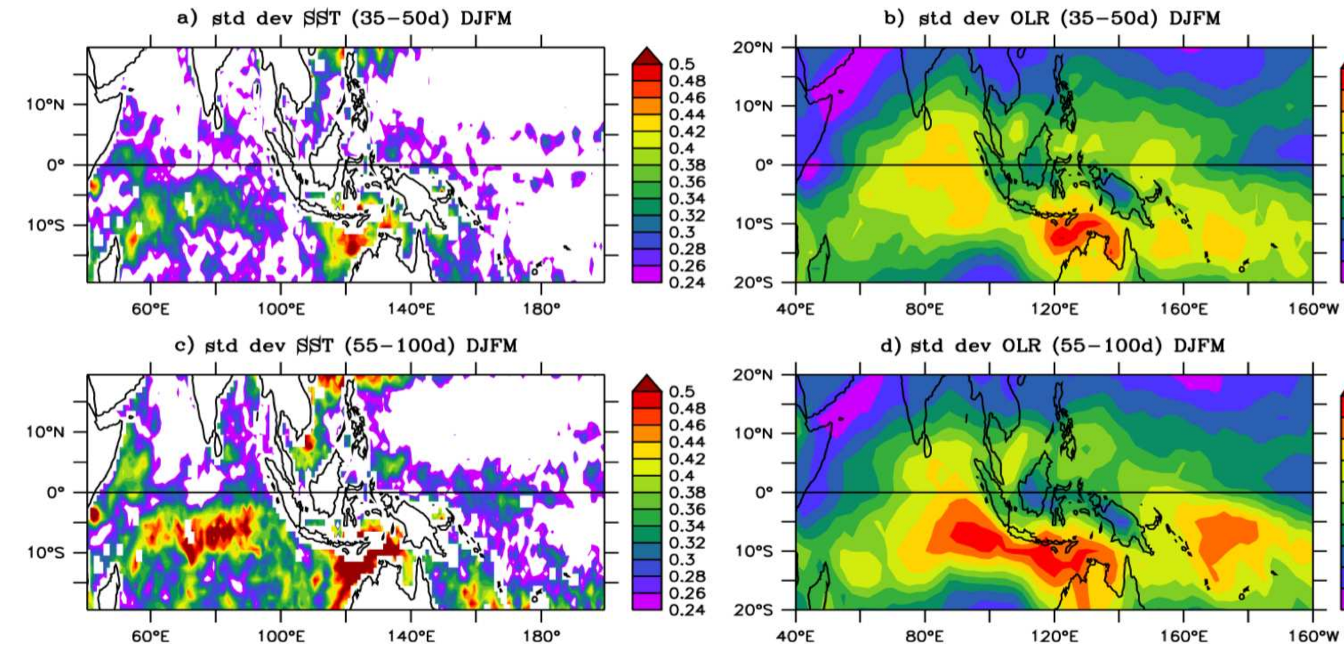

Fig. 3: maps of standard deviations of SST (TMI, left column; °C) and OLR (right column; W m^{-2}) for MJO HF (upper row) and LF (lower row) bands in DJFM.

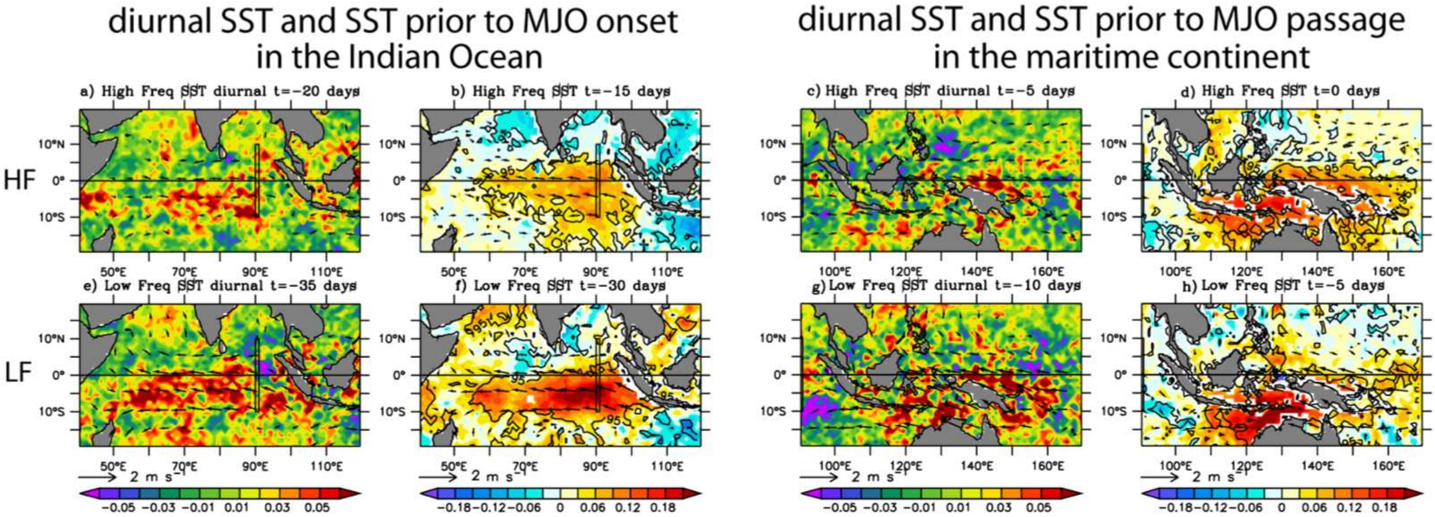

Fig. 4: difference between the HF (upper row) and LF (lower row) MJO composites, for SST diurnal amplitudes and daily SST, firstly prior to MJO onset in the Indian Ocean (left columns) and secondly prior to MJO propagation over the maritime continent (right columns). The weighted composites are at different lags for a negative intraseasonal OLR at 90°E, 10°N-10°S (location indicated by the black vertical bars) at t=0 in DJFM. SST diurnal amplitude and daily SST are shown about a quarter to eighter period before the OLR composites of figure 5. Surface winds are plotted for significance higher than 85%. Black contours show the 95% significant level.

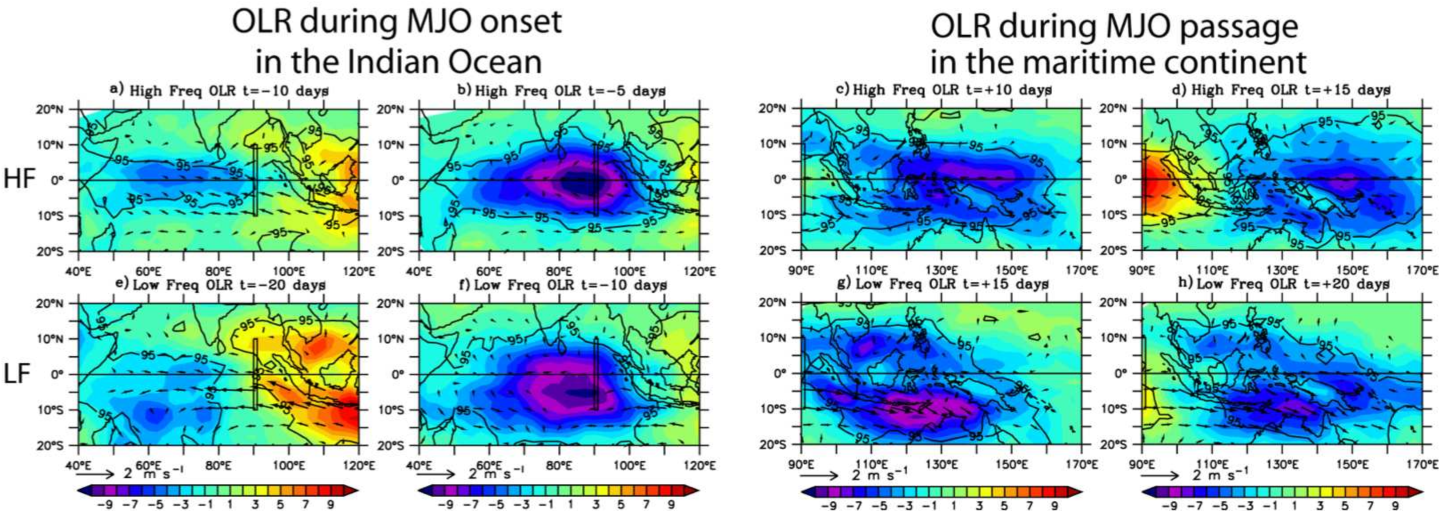

Fig. 5: similar to figure 4, but for OLR composites only, at various lags.

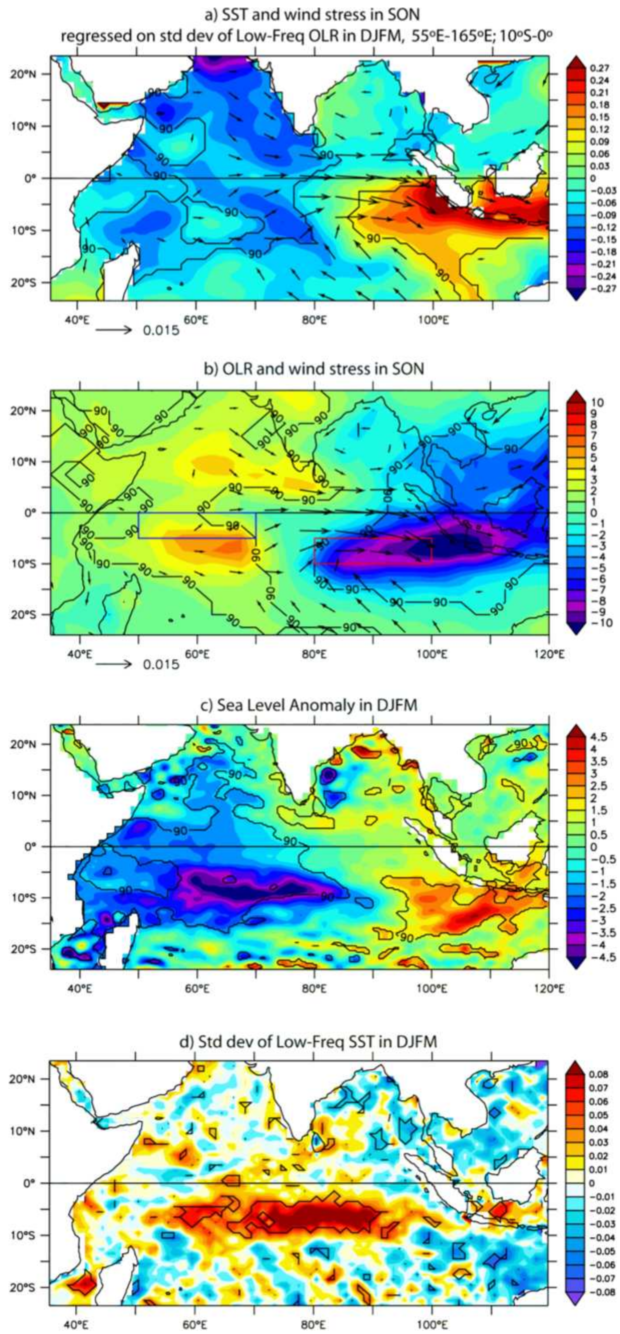

Fig. 6: ocean and atmosphere background state in boreal fall (SON) and winter (DJFM) regressed on southern LF-MJO activity in DJFM (OLR 55-100days, 55°E-165°E; 10°S-0º). (a): mean SST (°C, 1974-2007) and wind stress (N m^{-2}, 1987-2007) in fall (SON) before strong low-frequency MJO. (b): same as (a) but for OLR (color, W m^{-2}, 1974-2007). (c): for mean SLA in DJFM (cm, AVISO, 1992-2007). (d): for standard deviation of low-frequency SST in DJFM (TMI, 1998-2007). Surface winds are plotted for significance higher than 90%. The 90% significant level is added in black contours. The boxes defining the OLR-IOD index are shown in (b).

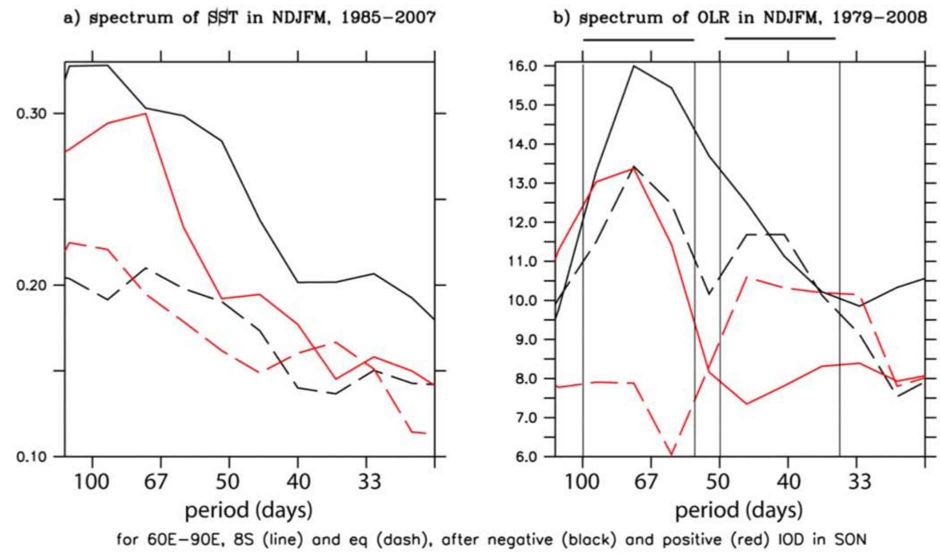

Fig. 7: same as Fig. 1, but for boreal winters following negative (black) and positive (red) IOD in fall.

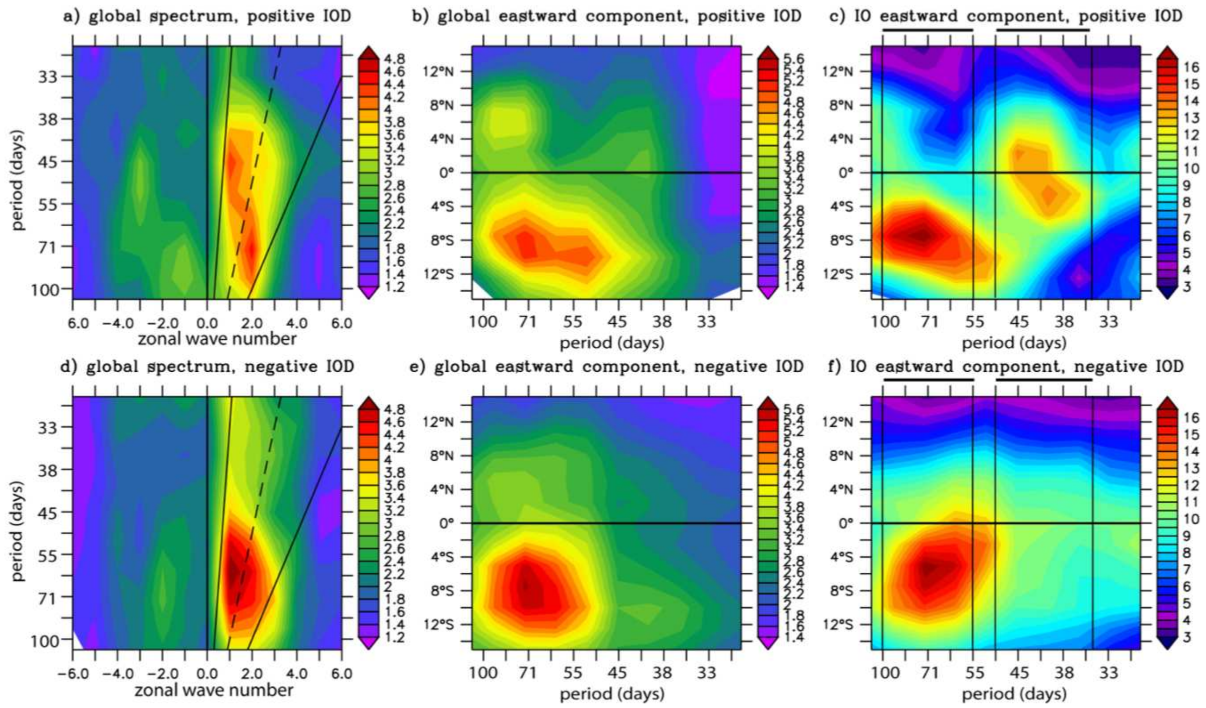

Fig. 8: longitude-time spectrum (left column), and latitudinal distribution of eastward propagating component globally (middle column) and in the Indian Ocean (right column), for OLR in DJFM, after positive IOD (upper row) and negative IOD (lower row) in SON (similar method to Fig. 2).

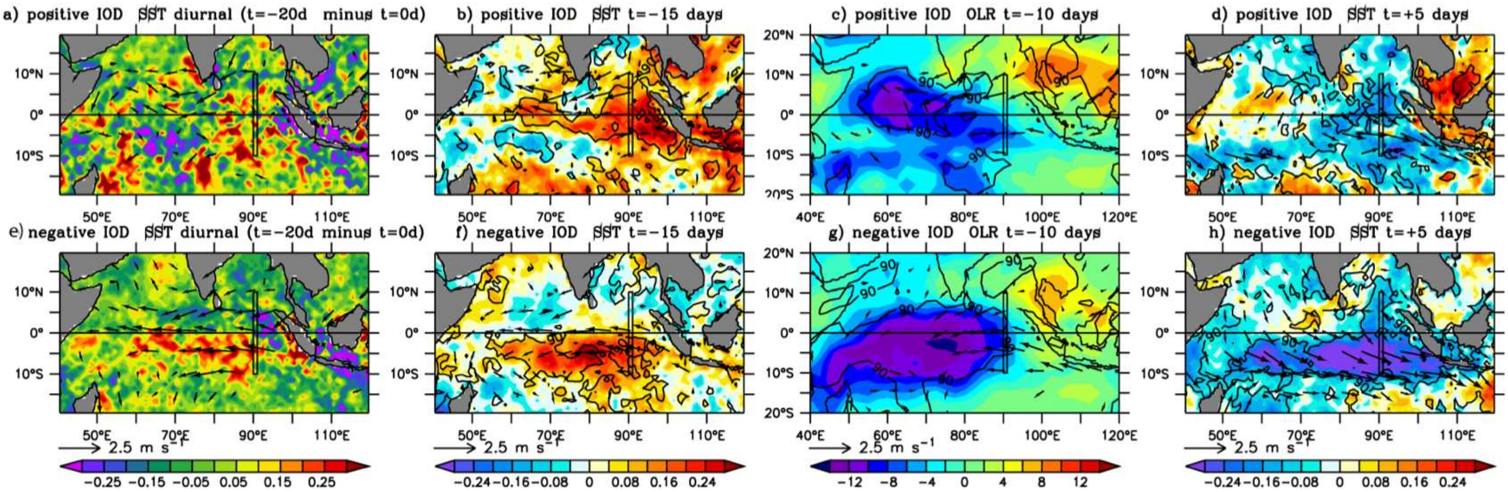

Fig. 9: MJO weighted composites in winter after positive (upper row) and negative (lower row) IOD conditions in fall: for SST (2nd column) and OLR (3rd column) intraseasonal anomalies during MJO onset, and for intraseasonal SST just after the passage of MJO active phase (4th column), in DJFM. Surface winds are plotted for significance higher than 85%. The 90% significant level is added in black contours. In the first column, the difference of the t=-20days and t=0 composites for the diurnal amplitude of SST (its total anomaly, no intraseasonal filtering) is plotted to remove the strong interannual signal (cf. fig. 11e,j), as the latter can not be trivially removed otherwise due to missing data constraints. The MJO index used here has been filtered in the broad 30-120days band, so as to let MJO timescale unconstrained *a priori* (see text for details).

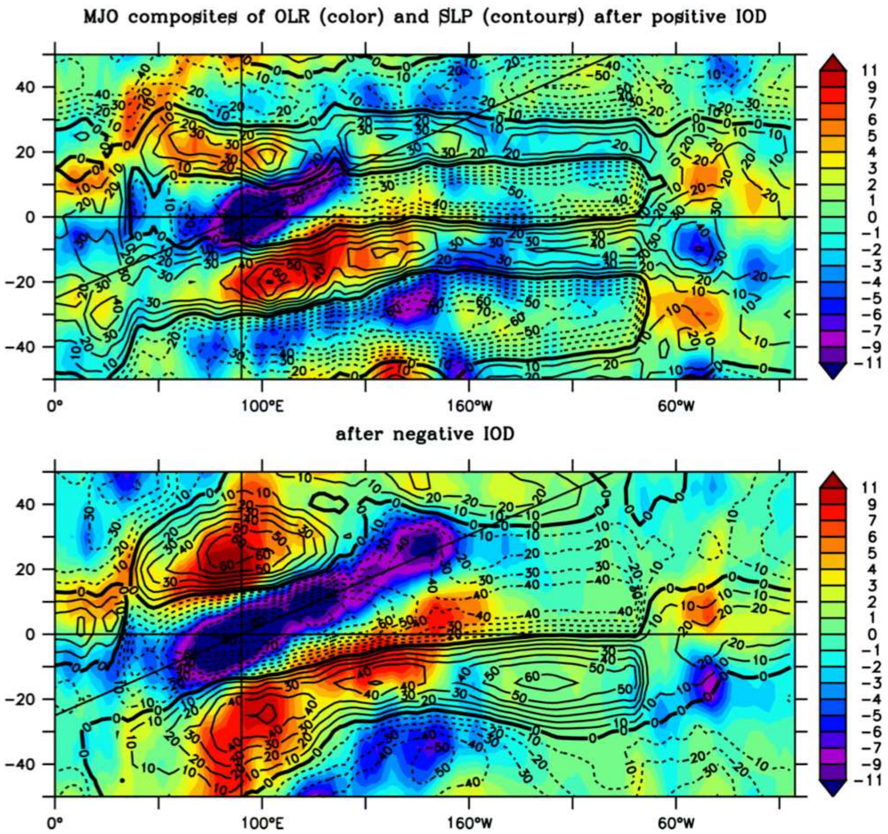

Fig. 10: time-longitude diagrams for lag-composites of OLR (color, to show MJO slow propagation in Indo-Pacific ITCZ-SPCZ) and SLP (contour, to evidence the circum-equatorial propagation as faster moist Kelvin waves), following different IOD conditions in fall: positive (upper) and negative (lower). The diagonal line shows the conventional MJO speed (5m/s). Latitudinal averaging is done over 15°S-5°N to capture the average propagation of MJO convection, shifted to the south during boreal winter. The fields composited here have not been high-pass filtered to limit time-aliasing. The MJO index used here is filtered over the broad 30-120days band, as in Fig. 9.

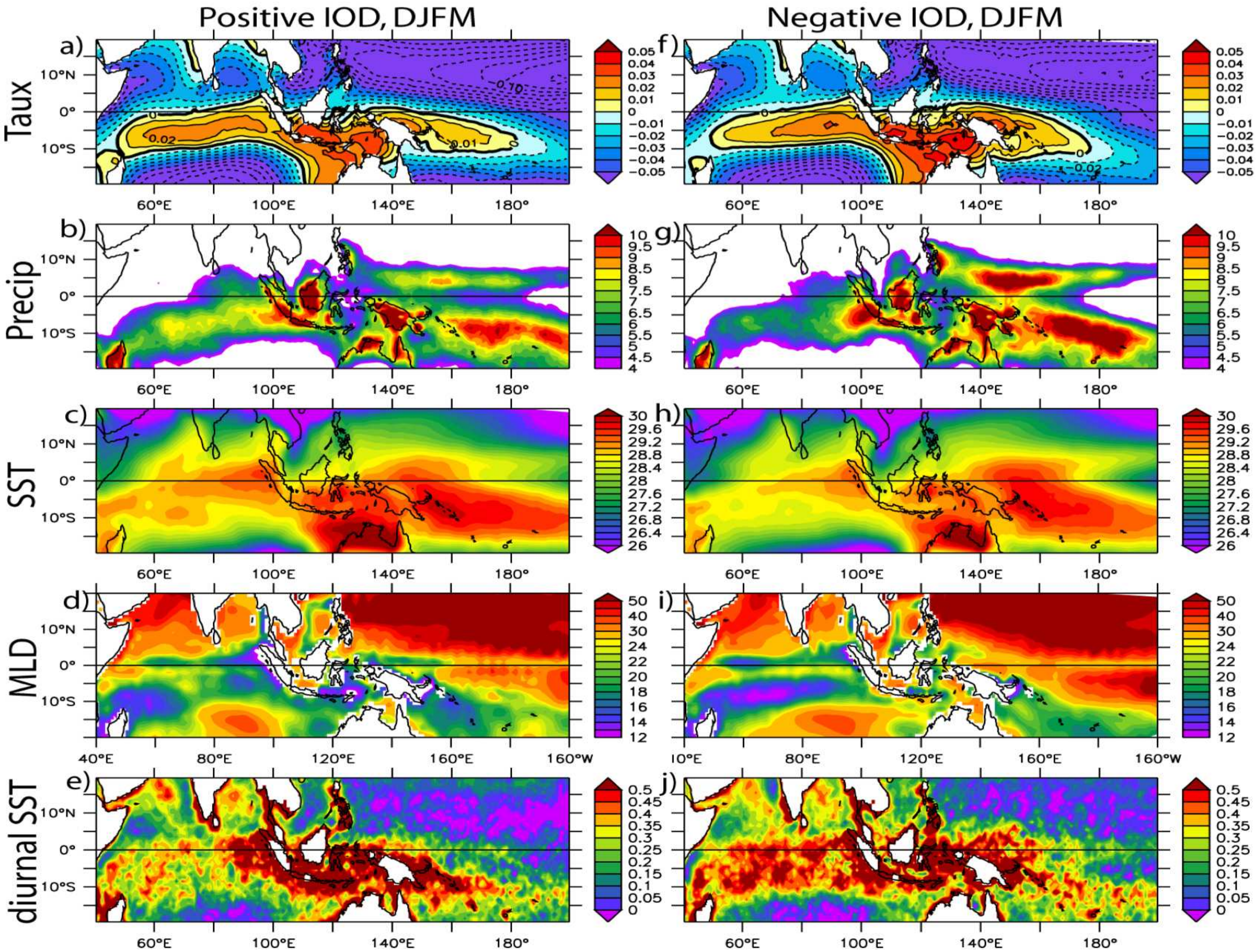

Fig. 11: Composites of mean DJFM state after positive (left column) and negative (right column) IOD. 1st line: zonal wind stress (SSMI/ERS1-2/Quikscat; N/m^2), 2nd line: precipitation (mm/d, GPCP), 3rd line: SST (°C, ERSST/Reynolds), 4th line: ocean mixed layer (m, from CERFACS-ENSEMBLES ocean reanalysis), 5th line: amplitude of SST diurnal cycle (°C, AVHRR). 7 (14) positive (negative) IOD events were used for the longest time series (1974-2007, SST, OLR and MLD). However, the shortest record (SST diurnal cycle) contains only 3 (7) positive (negative) events.